From modulational instability to focusing dam breaks in water waves

Félicien Bonnefoy [1], Alexey Tikan [2], François Copie [2], Pierre Suret,[2] Guillaume Ducrozet [1]
Gaurav Prabhudesai [3], Guillaume Michel [4], Annette Cazaubiel [5]
Eric Falcon [5], Gennady El [6] and Stéphane Randoux [2,*]

[1]*École Centrale de Nantes, LHEEA, UMR 6598 CNRS, F-44 321 Nantes, France*
[2]*Univ. Lille, CNRS, UMR 8523 - PhLAM - Physique des Lasers Atomes et Molécules,*
F-59000 Lille, France
[3]*Laboratoire de Physique de l'Ecole normale supérieure, ENS, Université PSL, CNRS, Sorbonne Université,*
Université Paris-Diderot, Paris, France
[4]*Sorbonne Université, CNRS, UMR 7190, Institut Jean Le Rond d'Alembert, F-75 005 Paris, France*
[5]*Université de Paris, Université Paris Diderot, MSC, UMR 7057 CNRS, F-75 013 Paris, France*
[6]*Department of Mathematics, Physics and Electrical Engineering, Northumbria University,*
Newcastle upon Tyne, NE1 8ST, United Kingdom

We report water wave experiments performed in a long tank where we consider the evolution of nonlinear deep-water surface gravity waves with the envelope in the form of a large-scale rectangular barrier. Our experiments reveal that, for a range of initial parameters, the nonlinear wave packet is not disintegrated by the Benjamin-Feir instability but exhibits a specific, strongly nonlinear modulation, which propagates from the edges of the wave packet toward the center with finite speed. Using numerical tools of nonlinear spectral analysis of experimental data, we identify the observed envelope wave structures with focusing dispersive dam break flows, a peculiar type of dispersive shock waves recently described in the framework of the semiclassical limit of the 1D focusing nonlinear Schrödinger equation (1D-NLSE). Our experimental results are shown to be in a good quantitative agreement with the predictions of the semiclassical 1D-NLSE theory. This is the first observation of the persisting dispersive shock wave dynamics in a modulationally unstable water wave system.

I. INTRODUCTION

Following the pioneering works by Whitham and Lighthill [1,2], Benjamin and Feir reported in 1967 the fundamental experimental and theoretical investigations of the time evolution of nonlinear deep-water surface gravity waves [3,4]. They demonstrated that a uniform continuous wave train is unstable with respect to small long-wave perturbations of its envelope, which may eventually lead to its disintegration after some evolution time [3–9]. In 1968 Zakharov showed that, for narrowband perturbations, the governing hydrodynamic equations can be reduced to a single equation for the complex wave envelope: the focusing one-dimensional nonlinear Schrödinger equation (1 D-NLSE) [10,11]. It was then understood that the instability, first observed in water waves, represents a ubiquitous phenomenon in focusing nonlinear media. Nowadays this phenomenon is called modulational instability (MI) and it has been observed and studied in many physical situations including plasma waves, matter waves, electromagnetic and optical waves [12–22].

---

*stephane.randoux@univ-lille.fr

According to the conventional picture, the early (linear) stage of MI is manifested in the exponential growth of all the perturbations of a plane wave background that fall in the region of the Fourier spectrum below a certain cutoff wave number. This simple classical (linear) picture provides a valid description of the process of the short-term destabilization of a plane wave of an infinite extent but it is inherently not adapted to the description of the nonlinear development of MI. Three distinct scenarios of nonlinear evolution of modulationally unstable wave systems described by the 1D-NLSE can be distinguished depending on the type of the initial condition considered. In the classical configuration (i) where the initial condition is a plane wave of infinite extent a particular scenario of the MI development strongly depends on the type of perturbation of the plane wave background that is considered. Breather solutions of the focusing 1D-NLSE are usually found to dominate the dynamics in this situation [23–31], although other nonlinear wave structures are also found depending on the localization and the solitonic content of the considered perturbation [32–36]. The destabilization of an infinite plane wave by a random perturbation leads to the emergence of a complex nonlinear wave structure associated with the so-called integrable turbulence [37] requiring statistical approaches to the description of the evolution of the nonlinear wave system [38–47].

There is another situation (ii) of physical relevance where the initial condition does not represent a plane wave of infinite extent but is a broad localized wave packet with a smooth envelope. In this situation, the initial evolution is dominated by nonlinear effects, and the classical MI (understood as an exponential growth of small long-wave initial perturbations) plays a secondary role. The dynamical evolution of such wave fields in nonlinear focusing dispersive media gives rise to generic dynamical features which are in sharp contrast with the conventional MI scenarios [48]. As shown in the optical fiber experiments reported in Ref. [49], the nonlinear focusing of such wave packets (light pulses) results in a gradient catastrophe that is regularized by dispersive effects through the universal mechanism yielding the local Peregrine soliton structure [48]. Note that these dynamical features have been observed in the nonlinear evolution of deep-water wave packets [50,51] even though they had not been connected to the universal semiclassical mechanism of the generation of the Peregrine soliton discussed in Ref. [48].

In a third configuration (iii), which is the main focus of the present paper, the initial field profile is characterized by sharp and significant amplitude changes. This configuration, which belongs to the class of the so-called Riemann problems [52], can give rise to dispersive shock waves (DSWs), a phenomenon that has attracted considerable attention in recent years but considered predominantly for stable media [53]. DSWs in *shallow water waves* (often termed *undular bores*) are a classical subject of fluid dynamics [54] with numerous contributions over the past 60 or so years [55], starting from the pioneering paper by Benjamin and Lighthill [56]. Note that some recent optical fiber experiments have demonstrated that light may evolve as a fluid, mimicking the features of undular bores or dispersive dam break flows in shallow water [57–59]. In contrast, there has been no experimental demonstration of the DSW dynamics on *deep water* so far.

In this paper, we present water wave experiments in which we demonstrate the persistent "focusing DSW" dynamics in the evolution of water wave packets of large extent and constant amplitude. Performing experiments in a long tank, we consider the evolution of nonlinear deep-water surface gravity waves having their envelope in the form of a large-scale rectangular barrier (a "box") of finite height. Our experimental observations reveal that, for a range of input parameters, the nonlinear wave train does not get disintegrated by the spontaneous MI but instead, exhibits a regular DSW type behavior that dominates the dynamics of the nonlinear wave at intermediate times.

More specifically, we observe that the initial sharp transitions between the uniform plane wave and the zero background undergo a very special nonlinear evolution leading to the emergence of two counter-propagating focusing dispersive dam break flows having the characteristic DSW structure, in good agreement with the scenario studied theoretically in Refs. [60,61] using semiclassical analysis of the focusing 1D-NLSE. We show that there exist ranges of parameters for which the dynamics observed in the experiment are nearly integrable and quantitatively agree with the theoretical predictions of Refs. [60,61]. We also show that the observed behaviors exhibit significant

degree of robustness to perturbative higher-order effects. Our paper presents the first observation of DSWs in deep water waves, supported by the previously developed semiclassical theory [60,61].

The paper is organized as follows. In Sec. II, we describe our experimental results obtained in a one-dimensional water tank. In Sec. III, we introduce the semiclassical formalism in which the observed dynamical behaviors can be interpreted. In Sec. IV, we perform quantitative comparison between experimental results and the semiclassical theory. In Sec. V, we show that the observed dynamics exhibits some degree of robustness to perturbative higher-order effects. A brief summary of our work is presented in Sec. VI together with a short discussion about possible perspectives.

II. WATER WAVE EXPERIMENT

The experiment was performed in a wave flume at the Hydrodynamics, Energetics, and Atmospheric Environment Lab (LHEEA) in Ecole Centrale de Nantes (France). The flume, which is 148 m long, 5 m wide, and 3 m deep, is equipped with a parabolic shaped absorbing beach that is approximately 8 m long. With the addition of pool lanes arranged in a W pattern in front of the beach the measured amplitude reflection coefficient is as low as 1%. Unidirectional waves are generated with a computer assisted flap-type wave maker. The setup comprises 20 equally spaced resistive wave gauges that are installed along the basin at distances $z_j = 6 + (j - 1)6$ m, $j = 1, 2, ...20$ from the wave maker located at $z = 0$ m. This provides an effective measuring range of 114 m.

In the first experimental run presented in Fig. 1(a), the wave maker produced one single large-scale wave packet having a near rectangular envelope. The duration ΔT_0 of the wave packet is $\sim$160 s. The water wave has a carrier period $T_0 = 2\pi/\omega_0$ of 0.87 s. The angular frequency ω_0 of the wave and the wave vector k_0 are linked according to the deep water dispersion relation $\omega_0^2 = k_0 g$ ($k_0 = 5.31$ m^{-1}, $\lambda_0 = 2\pi/k_0 \simeq 1.17$ m) with g the gravity acceleration. The amplitude of the generated envelope is $a_0 = 3.7$ cm implying that the wave steepness $k_0 a_0$ is $\simeq 0.19$ in this experiment.

In the second experimental run presented in Fig. 1(b), the computer controlled wave maker produced a sequence of three large-scale wave packets having rectangular envelopes. The three rectangular wave trains are individually generated over a global time interval of $\sim$220 s where they have increasing durations of $\Delta T_1 = 30$ s, $\Delta T_2 = 45$ s, $\Delta T_3 = 60$ s. The period of the carrier wave has been changed to $T_0 = 0.99$ s ($k_0 = 4.10$ m^{-1}, $\lambda_0 = 2\pi/k_0 \simeq 1.51$ m) and the amplitude of the generated envelope has been reduced to $a = 2$ cm which implies that the wave steepness $k_0 a = 0.082$ is 2.3 times smaller than in Fig. 1(a).

Figure 1(a) shows that disintegration of the large rectangular wave packet occurs as a result of modulational instability, in good agreement with experimental results previously reported in Refs. [4,5,8,9,62]. In particular, the initial destabilization of the plane wave background ($z < 40$ m) is associated with the exponential amplification of small random perturbations having frequency components falling in spectral regions of MI gain. We have checked that the amplification rate measured in our experiment is in agreement with the theory developed by Benjamin and Feir [3,4,46]. At long propagation distances ($z > 50$ m), the spectral (Fourier) analysis of the experimental wave train reveals a significant frequency down-shifting ($\sim$0.15 Hz at $z = 120$ m) correlated with a spectral broadening (see Fourier spectra plotted in the Supplemental Material [63]). These spectral features already observed in Ref. [8] demonstrate that the dynamical evolution reported in Fig. 1(a) is influenced by high-order nonlinear effects. Another clear signature of the presence of higher-order nonlinear effects lies in the fact that the front edge and the back edge of the wave train in Fig. 1(a) are propagating faster than the reference frame moving at the group velocity $\omega_0/(2k_0)$, a feature which is not observed in Fig. 1(b). Such a space-time evolution and the observed frequency down-shifting cannot be described by the 1D-NLSE but rather by other models like the unidirectional Zakharov equation or the Dysthe equation. The occurrence of higher-order nonlinear effects breaks the integrability of the wave system [see also Figs. 7(a)–7(d)] and it prevents the observation of any recurrence phenomenon, which represents an intrinsic feature of integrable wave systems.
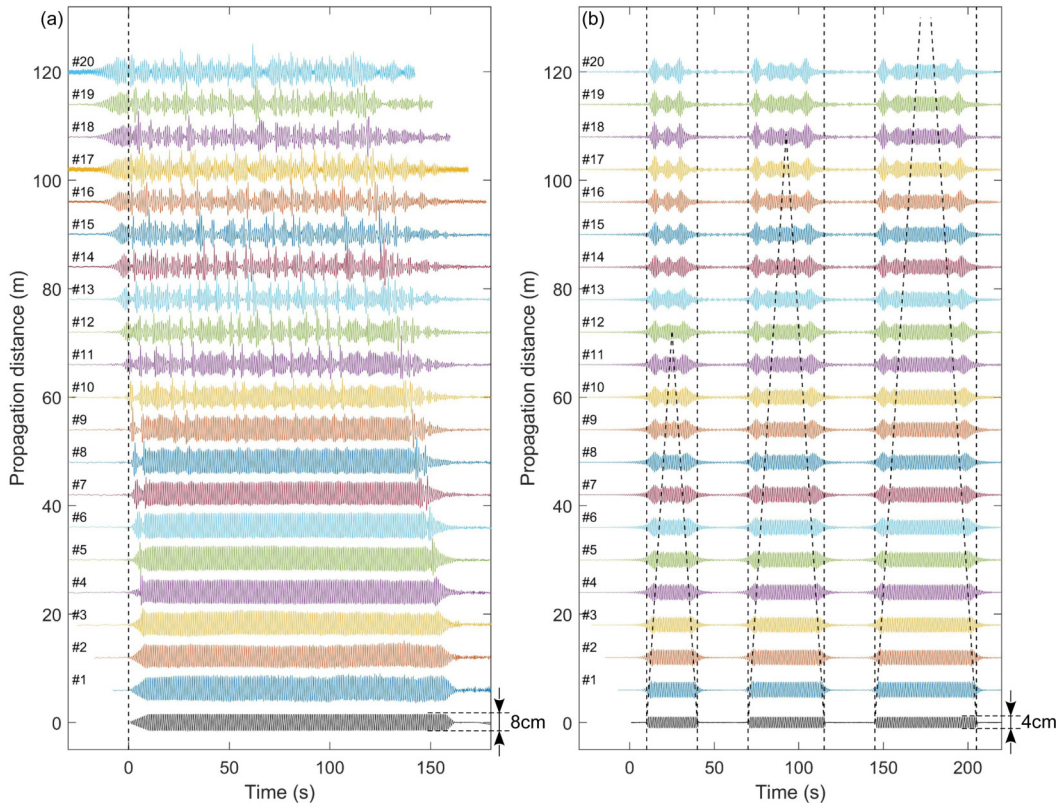
FIG. 1. Experimental results showing the nonlinear evolution of several rectangular wave trains along the 1D water tank. The evolution is plotted in the frame of reference moving at the group velocity $\omega_0/(2k_0)$ of the wave packets. (a) A large-scale wave packet of constant amplitude unstable to small perturbations of its envelope is disintegrated by the Benjamin-Feir instability [the wave steepness is $k_0 a_0 \simeq 0.19$, the carrier period is $T_0 = 0.87$ s and the wave amplitude is $a_0 = 3.7$ cm (see text)]. (b) Three "boxes" of constant identical amplitudes, which are not disintegrated by the Benjamin-Feir instability, undergo some strongly nonlinear modulation which propagates with finite speed from the front and back edges of the wave packet toward the center under the form of counter-propagating dispersive dam break flows with DSW structure [the wave steepness is 0.082, the carrier period is $T_0 = 0.99$ s and the wave amplitude is $a = 2$ cm (see text)]. The thick black dashed lines represent the theoretical breaking lines separating the genus 1 region from the genus 0 region; see calculation details in Secs. III B and IV A.

Figure 1(b) reveals that features of a qualitatively different nature occur at smaller steepness and for the rectangular wave packets having shorter durations. Each of the three generated rectangular wave packets qualitatively experiences some dispersive breaking following a scenario where two nonlinear wave trains generated from the edges of the rectangular envelopes counterpropagate toward the center of the box envelopes; see also the Supplemental Material Video S1 [63]. These two counterpropagating nonlinear wave trains were identified as two dispersive dam break flows in Ref. [60]. Remarkably, the relatively moderate steepness ($k_0 a \simeq 0.08$) characterizing water waves used in our experiment permits the clear observation of this phenomenon without the Benjamin-Feir instability significantly perturbes the wave dynamics.

Let us mention that some features qualitatively similar to those shown in Fig. 1(b) have been reported in Refs. [64,65] for water waves. In these experiments it was understood that the evolution of the unsteady wavefront was determined by combined influence of nonlinearity and dispersion but the degree of the analysis that was made did not exceed a very qualitative level.

In 2015, Shemer and Ee have reported some experiments showing the evolution of a truncated water wave train having a rectangular shape at initial time [66]. The physical values of parameters used in their experiments ($T_0 = 0.8$ s, $a = 2.6$ cm) are close to those used in the experiments that we report in Fig. 1(b). However, the truncated wave train considered by Shemer and Ee was weakly modulated in such a way that a Peregrine breather was generated after some propagation distance inside the water tank [66]. Even though the growth of large oscillations at the edges of the truncated wave train was reported, most of the study presented in Ref. [66] was focused on the build-up of the Peregrine breather generated in the central part of the rectangular wave train.

Interestingly our water wave experiments can be connected to the subject of diffractive focusing of waves in time and in space. In Ref. [67], Weisman *et al*. have reported an experiment where the envelope of a surface gravity water wave is modulated in time by a rectangular function. Near-field (Fresnel) diffraction patterns very similar to those observed in optics for light beams diffracted by a slit have been observed in the water wave context. Contrary to our experiment, the experiments reported in Ref. [67] are placed in a purely linear regime where (linear) diffraction of waves is observed. As it is clearly shown in Sec. IV, our experiments involve nonlinear wavefields that have some solitonic content. From an optical perspective, they are conceptually related to the subject of nonlinear diffraction of a field of constant amplitude by a slit in a focusing medium [68], a research topic introduced at theoretical level by Manakov [69,70].

Nonlinear diffraction of light beams in focusing media has been considered in a few optical experiments. The experiment reported in Ref. [71] has investigated diffraction from an edge in a self-focusing nonlinear photorefractive medium using a spatially incoherent light beam. In the very recent experimental work [72] the evolution of a 1D optical beam having a square profile was observed in a focusing photorefractive medium. While some of the robust qualitative features of the DSW dynamics predicted by the semiclassical 1D-NLSE theory [53] have been observed and interpreted in the context of the "topological control of extreme waves" [72], the quantitative comparison with the theory was limited because of the significant competition between the DSW dynamics and noise amplification in the modulationally unstable photorefractive medium.

Recent optical fiber experiments reported in Ref. [73] have also evidenced a spatio-temporal evolution very similar to the one that we observe with the rectangular wave train of the smallest width ($\Delta T_1 = 30$ s), compare Fig. 1(b) with Fig. 3(a) of Ref. [73]. However, the work reported in Ref. [73] was concentrated on the emergence of Peregrine-like events and did not allow for a meaningful quantitative, or even qualitative, identification of the observed wave patterns with DSWs due to very few oscillations observed.

III. DISPERSIVE FOCUSING DAM BREAK FLOWS: SEMICLASSICAL THEORY

The experimental results shown in Fig. 1(b) clearly indicate that the envelope of the wave packet develops oscillations with the typical period significantly smaller than the temporal extent of the wave packet. This separation of scales suggests the usefulness of an asymptotic WKB-type approach to the theoretical understanding of the arising dynamics. In this section, we show that the mathematical framework of dispersive hydrodynamics [74], a semiclassical theory of nonlinear dispersive waves, provides some insightful interpretation of the experimentally observed multiscale coherent structures.

A. The semiclassical framework

The experimental results reported in Fig. 1(b) can be interpreted within the framework of the focusing 1D-NLSE Eq. (2), written in a dimensional form as a spatial evolution equation

$$i\frac{\partial A}{\partial z} + \frac{k_0}{\omega_0^2}\frac{\partial^2 A}{\partial t^2} + \alpha k_0^3 |A|^2 A = 0, \tag{1}$$

TABLE I. Parameters corresponding to the three rectangular wave envelopes considered in our experiment ($k_0 = 4.1\,\mathrm{m}^{-1}$, $\omega_0 = 6.34\,\mathrm{s}^{-1}$, $a = 2.\,10^{-2}\,\mathrm{m}$, $\alpha = 0.91$). ϵ is the small dispersion parameter in Eq. (2). z_j^* represents the physical position at which the dispersive dam break flows collide. N represents the number of solitons embedded within the rectangular wave packets; see Sec. IV B.

ΔT_j (s)	L_{NL} (m)	L_D (m)	ϵ	z_j^* (m)	N
30	39.86	4414	0.095	74	3
45	39.86	9932	0.063	111	5
60	39.86	17658	0.047	148	7

where $A(z, t)$ represents the complex envelope of the water wave that changes in space z and in time t [75]. $\alpha = 0.91$ is a corrective term to the cubic nonlinear term. It has been introduced in Eq. (1) to take into account finite depth effects. In our experiment where the water depth h is 3 m, the numerical value of $k_0 h$ is ~ 12.3. This is large enough to consider that the condition of propagation in deep water regime is well verified but not large enough not to include some small corrective term in the nonlinear coefficient. A comprehensive discussion about the influence of finite depth effects on the values of linear and nonlinear coefficients is given in the Appendix.

In the experimental evolution reported in Fig. 1(b), the dynamics of the nonlinear wave is ruled by the interplay of two characteristic length scales associated with the temporal duration ΔT_j ($j = 1, 2, 3$) of the rectangular envelopes, namely, the nonlinear length $L_{NL} = 1/(\alpha k_0^3 a^2)$ and the linear dispersion length $L_D = (\omega_0 \Delta T_j)^2/(2 k_0) = g \Delta T_j^2/2$. Normalizing the propagation distance z along the flume as $\xi = z/\sqrt{L_{NL} L_D}$, the physical time as $\tau = t/\Delta T_j$, the complex field envelope as $\psi = A/a$, Eq. (1) takes the following dimensionless "semiclassical" form:

$$i\epsilon \frac{\partial \psi}{\partial \xi} + \frac{\epsilon^2}{2} \frac{\partial^2 \psi}{\partial \tau^2} + |\psi|^2 \psi = 0, \tag{2}$$

where $\epsilon = \sqrt{L_{NL}/L_D} \ll 1$ is a small dispersion parameter.

The numerical values of the physical and dimensionless parameters describing our experiment are reported in Table I for the three rectangular wave trains with temporal widths ΔT_j ($j = 1, 2, 3$). It can be easily seen that our experiments are always placed in a regime where $L_{NL} \ll L_D$ which implies that the experimental values of the ϵ parameter are much smaller than 1. Therefore our experimental observations can be interpreted within the mathematical framework of dispersive hydrodynamics [74], a semiclassical theory of nonlinear dispersive waves suitable for such multiscale coherent structures.

Equation (2) is considered with decaying data in the form of a rectangular barrier of finite height $q > 0$ and the width $2T$:

$$\psi(\tau, \xi = 0) = \begin{cases} q & \text{for} \quad |\tau| < T, \\ 0 & \text{for} \quad |\tau| > T. \end{cases} \tag{3}$$

We shall call the initial value problem Eqs. (2), (3) the 1D-NLSE box problem.

Figure 2(a) shows the numerical simulation of the 1D-NLSE box problem for $\epsilon = 0.04$; see also the Supplemental Material Video S2 [63]. Figure 2(a) provides evidence of a space-time evolution qualitatively similar to the one observed in our water wave experiment; see Fig. 1(b). In particular, the two nonlinear wave trains that are generated at the edges of the box counterpropagate toward the center of the box where they collide and produce a peak of large amplitude; see Fig. 2(d). Let us emphasize that simulations reported in Fig. 2 are done for an unperturbed box [see Eq. (3)]. If the box is perturbed by a small modulation or a small noise having frequency components falling within the MI gain curve, the perturbation will be amplified and an interaction between the DSWs generated
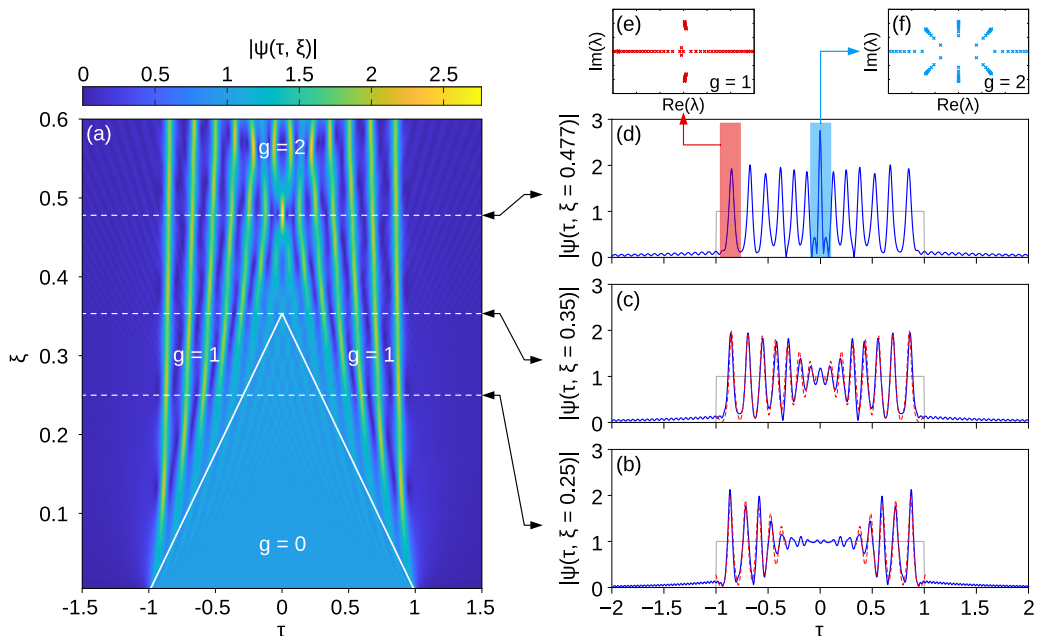
FIG. 2. Numerical simulation of Eq. (2) showing (a) the space time evolution of the wave field having a profile specified by Eq. (3) at $\xi = 0$ ($q = 1$, $T = 1$, $\varepsilon = 0.04$). The space-time evolution is separated into three regions of increasing genus g (see text). The genus $g = 0$ region corresponds locally to the plane wave solution. The genus $g = 1$ region is associated to DSWs that are generated from the edges of the box. The genus $g = 2$ region emerges from the collision of the two focusing dam break flows, see also the Supplemental Material Video S2 [63]. Curves plotted in blue lines in (b)–(d) represent the wave amplitude profiles at $\xi = 0.25$, $\xi = 0.35$, $\xi = 0.477$, respectively. Red dashed lines in (b) and (c) represent the amplitudes of the modulated cnoidal waves that are determined from Eqs. (5)–(7). (e), (f) Spectral (IST) portraits of isolated structures made at $\xi = 0.477$. The spectral portrait in (e) is mostly composed of two complex conjugate bands demonstrating that the analyzed structure has a genus $g = 1$ (solitonlike structure, see text). The spectral portrait in (f) is composed of three bands demonstrating that the genus of the analyzed structure is $g = 2$ (breatherlike structure).

from the edges of the box and the coherent structures seeded by the initial perturbation will be observed. The study of the associated dynamics represents an interesting perspective of our work.

Note that the typical scale of the coherent structures found in the dam break flows is around $\sim \epsilon \ll T$; see Figs. 2(b)–2(d). Note also that the dynamics reported in Fig. 2(a) is not influenced by the exact shape of the field near the edges of the box. Space-time evolutions similar to the one reported in Fig. 2(a) are observed as long as the typical space scale of the transition between the zero and the constant backgrounds is of the order of ϵ.

B. Main results from the semiclassical theory

In this section, we summarize some important theoretical results about the 1D-NLSE box problem. The quantitative comparison between these theoretical results and the experimental results will be presented in Sec. IV.

First, it is instructive to use the Madelung transform $\psi = \sqrt{\rho(\tau, \xi)} \exp[i\epsilon^{-1} \int^{\tau} u(\tau', \xi) d\tau']$ to represent the 1D-NLSE in the dispersive hydrodynamic form

$$\rho_\xi + (\rho u)_\tau = 0,$$

$$u_\xi + u u_\tau - \rho_\tau - \varepsilon^2 \left(\frac{\rho_\tau^2}{8\rho^2} - \frac{\rho_{\tau\tau}}{4\rho} \right)_\tau = 0, \tag{4}$$

where ρ and u are analogues of the fluid depth and velocity respectively. Within the hydrodynamic interpretation [Eq. (4)], the box initial data [Eq. (3)] can be viewed as a combination of two hydrodynamic dam breaks (i.e., step transitions from finite depth $\rho = q^2$ to "dry bottom" $\rho = 0$) of opposite polarities, placed at the distance $2T$ from each other. It is important to stress that the 1D-NLSE "fluid" here has nothing to do with the underlying water wave context of the original problem; moreover, due to the focusing nature of the 1D-NLSE Eq. (2), the classical "pressure" term in the hydrodynamic representation Eq. (4) is negative.

The dispersive hydrodynamic representation Eq. (4) provides an important insight into the 1D-NLSE evolution of different types of initial data. Linearizing system Eq. (4) about a constant equilibrium flow $\rho = \rho_0$, $u = 0$ (a plane wave of the 1D-NLSE) one obtains the usual 1D-NLSE dispersion relation $\omega = \pm k\sqrt{(\varepsilon k)^2 - 4\rho_0}$ implying modulational instability of plane waves for long enough waves with $\varepsilon k < 2\sqrt{\rho_0}$. This is the classical Benjamin-Feir instability, which is manifested as a dispersion-dominated, linear wave phenomenon *within 1D-NLSE*. The initial exponential growth of harmonic, long-wave perturbations is mediated by nonlinearity leading to the formation of Akhmediev breathers or more complicated breather structures associated with integrable turbulence [76,77].

The focusing 1D-NLSE dam break problem Eqs. (2) and (3) is rather special in the sense that it triggers both nonlinearity and dispersion in Eq. (4) from the early time of the evolution. As a result, it leads to the formation of a coherent, unsteady nonlinear wave structure that is very different from those arising in the development of the BF instability or in the evolution of broad smooth humps. This structure can be viewed as a focusing counterpart of the well-known dispersive-hydrodynamic phenomenon, called a dispersive shock wave (DSW) [53], which represents an expanding, nonlinear wave train connecting two disparate constant fluid states. DSW is described by a slowly modulated, locally periodic wave solution of a dispersive equation (1 D-NLSE in our case) gradually transforming from a soliton at one edge to a vanishing amplitude, harmonic wave at the opposite edge. The special modulation providing such a transition has been found in Ref. [78] as a self-similar solution of the Whitham modulation equations [54] associated with the 1D-NLSE. Typically, DSWs are the features of stable media, described by such equations as the KdV or defocusing NLS equations (see Ref. [53] and references therein) but for a special Riemann data (dam break) the DSWs can be generated in unstable (focusing) media [60,79,80]. The persistence of DSW dynamics in focusing dam break problem is due to a special "hyperbolic" modulation as explained below.

The periodic solutions of the focusing 1D-NLSE are known to be modulationally unstable with respect to small initial perturbations (see, e.g., Ref. [81]), but this modulational instability is more subtle than the BF instability of a plane wave. It turns out that the instability of nonlinear periodic solution can be "inhibited" by a special modulation yielding a "hyperbolic" wave behavior characterized by finite speeds of propagation. This modulation is described by a similarity solution of the Whitham modulation equations associated with the 1D-NLSE [82,83] and it is exactly the modulation that is realized in the dispersive regularization of the dam break flow in the focusing 1D-NLSE and enables the persistent DSW structure that can be observed in an experiment.

The box problem Eqs. (2) and (3) has been studied analytically in Refs. [60,61] using a combination of the Whitham modulation theory and an IST-based Riemann-Hilbert problem approach [84]. The theoretical developments of Ref. [60] important for the interpretation of our experimental results in water waves can be conveniently explained by considering Fig. 2, where the numerical simulation of the focusing dam break problem for the 1D-NLSE equation is presented along with the results of the so-called "local IST" analysis [77] of the emerging wave structures [Figs. 2(e) and 2(f)]. The plots in Figs. 2(e) and 2(f) show the qualitative changes of the nonlinear (IST) spectra occurring in the course of the wave propagation. These spectra and the associated nonlinear waves are characterized by a fundamental integer index g called genus which enables classification of the emerging wave structures in terms of the number $N = g + 1$ of "nonlinear

Fourier modes" involved. The genus itself characterises topology of the hyperelliptic Riemann surfaces associated with the special class of the 1D-NLSE solutions, called finite-gap potentials (see, e.g., Refs. [75,85]). As shown in Ref. [60] the solutions of the semiclassical 1D-NLSE box problem can be asymptotically described by slowly modulated finite-gap 1D-NLSE solutions with the genus changing across certain lines in τ-ξ plane called *breaking curves*. In particular, the wave structures regularizing the initial dam breaks at $\tau = \pm T$ in the box problem have genus $g = 1$ while the genus 2 structures emerge as a result of the interaction of two counter-propagating dispersive dam break flows having the signature structure of dispersive shock waves (DSWs) [53].

The asymptotic solution of the box problem for the small dispersion 1D-NLSE Eq. (2) has different form in different regions of τ-ξ plane (see Fig. 2). For $\xi < \xi^*$, where $\xi^* = \frac{T}{2\sqrt{2}q}$ the solution represents two counter-propagating focusing DSWs—seen as the genus one regions in Fig. 1—connecting two disparate genus zero states: the "dry bottom" state $\psi = 0$ at $|\tau| > T$ and the constant state $\psi = q$ for $(2\sqrt{2}q\xi - T) < \tau < (-2\sqrt{2}q\xi + T)$. The local structure of both DSWs is described by the elliptic ("cnoidal") solution of the 1D-NLSE,

$$\rho = (q + b)^2 - 4qb\,\mathrm{sn}^2(2\sqrt{qb/m}\,(\tau - a\xi - \tau_0)\varepsilon^{-1}; m), \tag{5}$$

where $\mathrm{sn}(\cdot)$ is a Jacobi elliptic function with the modulus $m \in [0, 1]$ given by

$$m = \frac{4qb}{a^2 + (q + b)^2}.$$

The modulation parameters $a(\tau, \xi)$, $b(\tau, \xi)$ are found from equations

$$a = \pm\frac{2q}{m\mu(m)}\sqrt{(1 - m)[\mu^2(m) + m - 1]},$$

$$b = \frac{q}{m\mu(m)}[(2 - m)\mu(m) - 2(1 - m)], \tag{6}$$

$$\frac{\tau \mp T}{\xi} = \pm\frac{2q}{m\mu(m)}\sqrt{(1 - m)(\mu^2(m) + m - 1)}\left(1 + \frac{(2 - m)\mu(m) - 2(1 - m)}{\mu^2(m) + m - 1}\right), \tag{7}$$

where $\mu(m) = E(m)/K(m)$. $K(m)$ and $E(m)$ are the complete elliptic integrals of the first and second kind respectively. The signs $\pm$ in Eqs. (6) and (7) correspond to right- and left-propagating waves. The initial position τ_0 in Eq. (5) is given by $\tau_0 = \pm T$. In practice, τ_0 depends on the way the sharp edges of the "box" are smoothed in the experimental signal or in numerical simulations so for a practical comparison with the theory, one chooses τ_0 by fitting to the experimental/numerical data.

Solution Eqs. (5)–(7) describe two symmetric oscillatory structures exhibiting the fundamental 1D-NLSE solitons ($m = 1$) with the amplitude $|\psi_m| = 2q$, located at $\tau = \pm T$. The structures degenerate, via the modulated elliptic regime, into the vanishing amplitude linear wave ($m = 0$) at the internal moving edges propagating toward the box center with constant velocities $\pm2\sqrt{2}q$. The solutions computed from Eqs. (5)–(7) are plotted with red dashed lines in Figs. 2(b) and 2(c). Very good quantitative agreement is found between these theoretical solutions and numerical simulations of the 1D-NLSE [blue lines in Figs. 2(b) and 2(c)]. Let us recall, for the sake of clarity, that the theoretical and numerical solutions discussed here represent the envelopes (modulations) of wave packets plotted in Fig. 1(b).

The equation of the first breaking curve Γ_1 separating the genus $g = 0$ region from the genus $g = 1$ region in the diagram in Fig. 2(a) is

$$\Gamma_1: \quad \xi = \frac{T - |\tau|}{2\sqrt{2}q}. \tag{8}$$
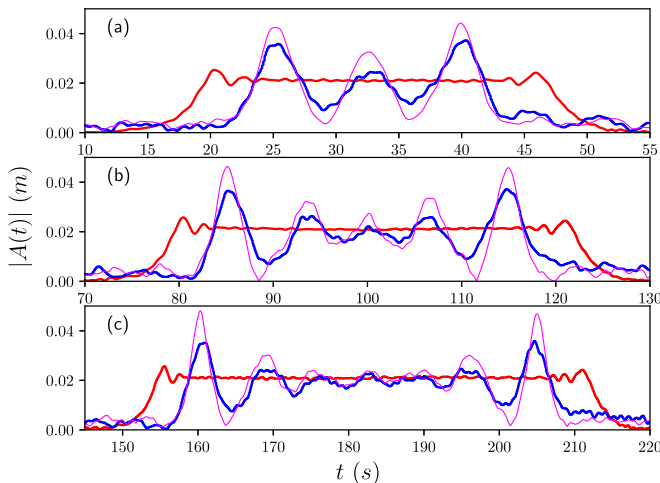
FIG. 3. Modulus of the water wave envelopes with durations (a) $\Delta T_1 = 30$ s, (b) $\Delta T_2 = 45$ s, (c) $\Delta T_3 = 60$ s. The red (respectively, blue) lines represent the experimental envelopes of the signal recorded at $z_1 = 6$ m (respectively, $z_{20} = 120$ m), close to (respectively, far from) the wave maker. The magenta lines represent the envelopes computed from the numerical simulation of Eq. (1) ($k_0 = 4.1$ m^{-1}, $\omega_0 = 6.34$ s^{-1}, $\alpha = 0.91$) by taking as initial condition the complex envelope measured by the gauge closest to the wave maker (red lines, $z_1 = 6$ m).

Equation (8) yields the DSW collision time $\xi^* = \frac{T}{2\sqrt{2}q}$ corresponding to Fig. 2(c). For $\xi > \xi^*$ the region with $g = 2$ is formed, confined to another breaking curve [not shown in Fig. 2(a)]. One of the prominent features of the genus 2 region is the occurrence of a large-amplitude breather at the center with the characteristics close to those of the Peregrine soliton [see Fig. 2(d)] as predicted in Ref. [60] and experimentally observed in fiber optics in Ref. [73].

We now demonstrate that deep water waves, while providing the classical example of the Benjamin-Feir instability, present also a medium supporting the "hyperbolic" dispersive dam break (DSW) scenario of the wave-packet evolution for a range of input parameters. This is done in Sec. IV by a quantitative comparison of the water wave experiment with the modulated 1D-NLSE solution [60] and the "local IST" analysis of the experimentally observed wave patterns [77,86], confirming the spectral topological index (genus) of generated waves.

IV. DATA ANALYSIS AND COMPARISON WITH THE THEORY

A. Numerical simulations of the 1D-NLSE, breaking lines, collision points, and modulated cnoidal waves

In this section, we focus on the quantitative comparison between experimental results and the semiclassical theory. First we have performed numerical simulations of Eq. (1) by taking as initial condition the complex envelope $A(z_1, t)$ of the signal measured by the gauge closest to the wave maker ($z_1 = 6$ m). The complex envelope has been computed from the experimentally-recorded signals by using standard techniques based on the Hilbert transform, as discussed, e.g., in Ref. [75]. Figure 3 shows the modulus $|A(z_{20}, t)|$ of the complex envelope that is computed at $z_{20} = 120$ m, the position where is located the gauge furthest from the wave maker. The agreement between the experimental results and the numerical simulations is quantitatively good for each of the three generated rectangular wave trains.

As a first valuable test of the theory introduced in Sec. III, we plot the linear breaking curves separating the genus 0 (plane wave) regions from the genus 1 (DSW) regions. Rephrasing Eq. (8)
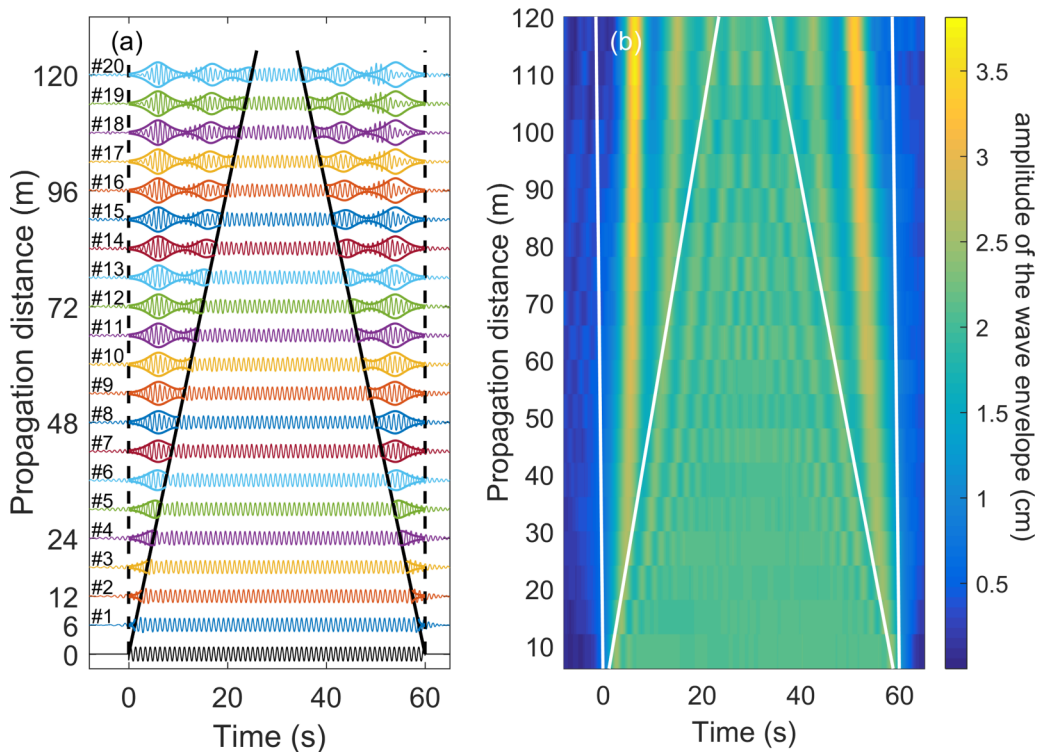
FIG. 4. Experimental results showing the nonlinear evolution of the rectangular wave packet of largest size ($\Delta T_3 = 60$ s, $a = 2$ cm, $k_0 a = 0.082$, $T_0 = 0.99$ s) in Fig. 1(b). (a) Signals recorded by the 20 gauges placed all along the tank. All the envelopes superimposed on the carrier wave are computed from solutions given by Eqs. (5)–(7) using $\tau_0 = -0.48$. The breaking lines plotted with full black lines in (a) are computed from Eq. (8). (b) Space-time evolution of the modulus of the envelope of the experimental signals. The white lines in (b) represent the breaking curves computed from Eq. (8).

in physical units, we easily find that the slopes $s_\pm$ of the breaking lines in the z-t plane read $s_\pm = \pm \omega_0/(4 a \sqrt{\alpha} k_0^2)$ and that the collision between the two counterpropagating dam break flows occurs at the position $z_j^* = \omega_0 \Delta T_j/(8 a \sqrt{\alpha} k_0^2)$.

The numerical values of the positions at which the collisions between the counterpropagating dam break flows occur are summarized in Table I for the three boxes generated in our experiment. The breaking lines separating the genus 0 region from the genus 1 region are plotted in Fig. 1(b). It can be readily seen that there is a good quantitative agreement between theoretical and experimental results. In particular, the distance at which the collision is predicted to occur for the largest box is larger than the physical length of the water tank and it is clear that the collision between the dam break flows is not experimentally observed in this situation; see Fig. 1(b) and also Fig. 4.

To go one step further in the analysis of our experiment, we now compare experimental data with the modulated cnoidal solution that has been discussed in Sec. III. To this end Eqs. (5)–(7) are solved and rephrased to physical variables according to the transformations introduced in Sec. III A. Considering only the box of largest size where the counterpropagating dam break flows are the most developed near the end of the water tank ($z \sim 120$ m), Fig. 4 shows that the modulated cnoidal wave envelope determined from the semiclassical theory matches quantitatively well the experimental results over the whole range of evolution of the dam break flows (i.e., from $z = 6$ m to $z = 120$ m). The numerical value of τ_0 has been determined from the signal measured at the last gauge, at $z_{20} = 120$ m ($\tau_0 = -0.48$).
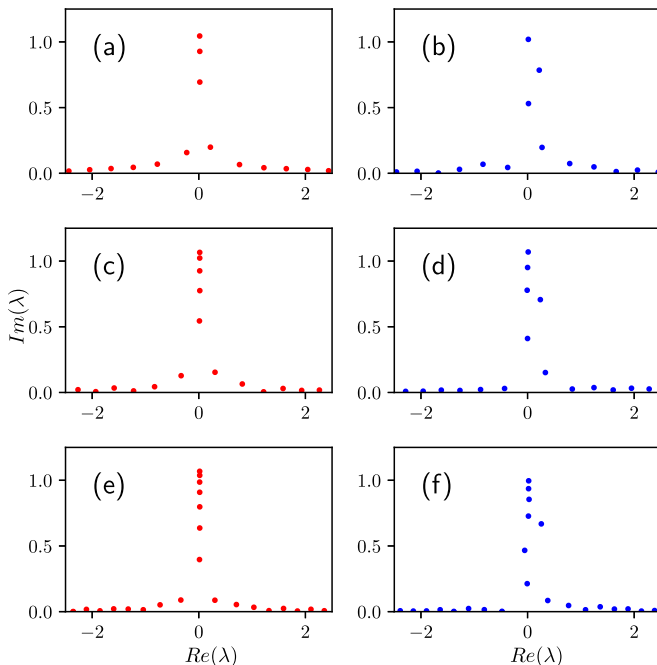
FIG. 5. Discrete IST spectra of the three envelopes measured at $z_1 = 6$ m (Left column) and $z_{20} = 120$ m (Right column). (a), (b) $\Delta T_1 = 30$ s, (c), (d), $\Delta T_2 = 45$ s, (e), (f) $\Delta T_3 = 60$ s. Only the upper half part of the complex plane is represented.

B. Inverse scattering transform analysis of the experimental data

Some other insights into our experimental results can be obtained from the perspective of the inverse scattering transform (IST) method. The configuration considered in our experiments corresponds to the initial value problem specified by Eqs. (2) and (3). As shown by Zakharov and Shabat [87], the nonlinear dynamics in this kind of problem is determined by the IST spectrum that is composed of two components: a discrete part related to the soliton content of the box data and of a continuous part related to the dispersive radiation. In particular, it is known that the number N of solitons embedded inside the initial box is given by $N = \text{int}(1/2 + 1/(\pi \epsilon))$, where $\text{int}(x)$ denotes the integer part of x [69,70,88–90].

As shown in Table I, the number of solitons that are embedded inside the rectangular wave trains is predicted to grow from $N = 3$ for the smallest box ($\epsilon = 0.095$) to $N = 7$ for the largest box ($\epsilon = 0.047$). To check this result from experimental signals and to investigate more in depth the integrable nature of the features experimentally observed, we now consider the non-self-adjoint Zakharov-Shabat eigenvalue problem,

$$\epsilon \frac{d\mathbf{Y}}{d\tau} = \begin{pmatrix} -i\lambda & \psi_0 \\ -\psi_0^* & i\lambda \end{pmatrix} \mathbf{Y}, \tag{9}$$

which is associated with Eq. (2). $\mathbf{Y}(\tau; \lambda, \epsilon)$ is a vector where $\lambda \in \mathbb{C}$ represent the eigenvalues composing the discrete spectrum associated with the soliton content of the complex envelope ψ_0 measured at some given propagation distance. Note that the linear spectral problem Eq. (9) can be identified as one half of the Lax pair for Eq. (2) [91].

Figure 5 shows the complex eigenvalues λ that are computed from the numerical resolution of Eq. (9) made by using the Fourier collocation method described and used, e.g., in Ref. [77,86,91]. For the sake of clarity only the upper part of the complex plane is represented but complex conjugate

eigenvalues are obviously obtained from the numerical resolution of Eq. (9). Figure 5 (left column) shows the complex eigenvalues computed for the three experimental envelopes (red lines in Fig. 3) measured at $z_1 = 6$ m, close to the wave maker. Remarkably, nearly all of the nonzero eigenvalues numerically computed are distributed close to the vertical imaginary axis, demonstrating that the solitons embedded inside the three rectangular wave trains have negligible velocity at the initial time. In fact, the rigorous semiclassical IST analysis of the box problem [61] shows that the discrete spectrum is located on the imaginary axis as $\epsilon \to 0$. The number of discrete eigenvalues found from numerical IST analysis and reported in Figs. 5(a), 5(c), and 5(e) is in good agreement with results reported in Table I.

Figure 5 (right column) shows the complex eigenvalues that are computed for the three experimental envelopes (blue lines in Fig. 3) measured at $z_2 = 120$ m, far from the wave maker. In the IST theory of the 1D-NLSE, these discrete eigenvalues do not change in the evolution time. In the experiment, we find that this isospectrality condition is not perfectly verified because of the unavoidable occurrence of small perturbative effects. It is, however, clear that the number of eigenvalues is preserved over the propagation distance characterizing our experiment, i.e., between $z_1 = 6$ m and $z_2 = 120$ m. Moreover the global shape of the IST spectra is well preserved (compare left and right columns in Fig. 5), thus confirming the nearly integrable nature of the features observed in the experiment.

Note that the degree of preservation of the eigenvalues reported in Fig. 5 was not reached in our initial preliminary experiments because of the occurrence of a slightly multimodal propagation in the water tank. Such a multimodal propagation is prone to occur because the width of the tank (5 m) is relatively large as compared to the typical experimental wavelength (~ 1 m). Therefore, we have taken great care that the motion of the wave maker effectively produces nearly a single-mode excitation leading to a dominant 1D wave propagation.

V. WATER WAVE EXPERIMENT: ROBUSTNESS OF THE OBSERVED DYNAMICS TO HIGHER-ORDER EFFECTS

A. Space-time evolution

In this section, we demonstrate that the observed dynamics exhibits some degree of robustness to higher-order effects that unavoidably perturb the wave evolution when experimental parameters are changed in such a way that the strength of nonlinearity increases. To do so, we have simply increased the frequency of the wave maker from $f_0 = 1/T_0 = 1.01$ Hz to $f_0 = 1.28$ Hz while also decreasing the amplitude of the wave envelope from 2 cm to 1.4 cm. With these changes, the nonlinear length decreases from $L_{NL} = 39.86$ m to $L_{NL} = 18.77$ m while the linear dispersive lengths L_D remain unchanged and identical to those summarized in Table I.

Figure 6 shows the space-time evolutions of the three rectangular envelopes that are observed in this situation where the nonlinearity strength is increased, see also the Supplemental Material Video S3 [63]. Contrary to the experimental space-time evolutions considered in Secs. II and IV, there is now a marked asymmetry in the space evolution of the three wave packets. Even though frequency down-shifting is not observed in the studied regime, a significant spectral broadening phenomenon is found to occur, see Fourier spectra plotted in the Supplemental Material [63]. As discussed in detail in Sec. V B, integrability of the wave system is not preserved in this regime where higher-order nonlinear effects influence the wave dynamics. In these conditions, the observed dynamics is not described by the 1D-NLSE but rather by other models like the unidirectional Zakharov equation or the Dysthe equation [50]. Note that small higher-order effects are already noticeable in the details of Fig. 4(a) where the envelope of the modulated cnoidal wave fits better the left part than the right part of the wave packet at large distances from the wave maker.

Despite the undisputable presence of higher-order nonlinear effects in water wave experiments reported in Fig. 6, it is clear that the scenario of emergence of counter-propagating dispersive dam break flows remains qualitatively well observed. White lines plotted in Fig. 6 represent the
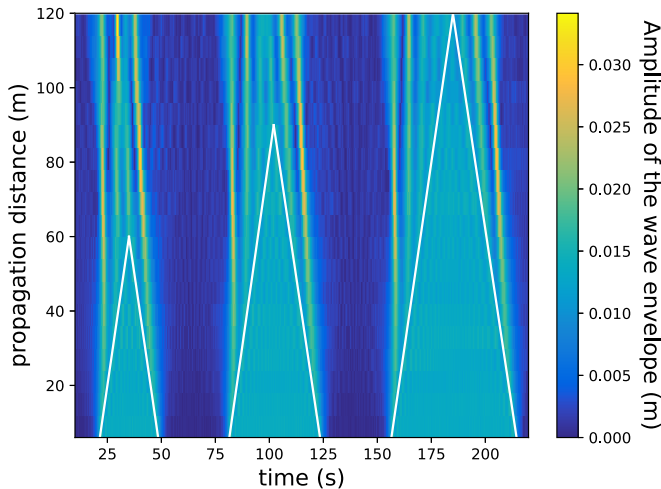
FIG. 6. Space-time evolution of the envelopes of three rectangular wave packets ($\Delta T_1 = 30$ s, $\Delta T_2 = 45$ s, $\Delta T_3 = 60$ s) in the regime where higher-order nonlinear effects have a perturbative influence. The carrier frequency $f_0 = 1/T_0$ is 1.28 Hz. Other experimental parameters are $k_0 = 6.58$ m^{-1}, $a = 0.014$ m (the wave steepness is $k_0 a = 0.09$). White lines represent breaking curves that are determined using the methodology described in Sec. IV A.

breaking lines that are computed from the semiclassical theory presented in Sec. III [see Eq. (8)]. At a qualitative level, the breaking lines still clearly separate regions where DSWs (genus 1) are found from regions where the (unmodulated) plane waves (genus 0) are found. Therefore, these breaking lines retain some relevance to the description of the dynamics, even in the presence of perturbative higher-order effects.

B. Nonlinear spectral analysis

In the regime where higher-order nonlinear effects influence the dynamics, the wave system is no longer described by the 1D-NLSE and rigorously speaking, the dynamics is no longer of an integrable nature. However, mathematical tools of nonlinear spectral analysis can still be used to advantage for getting relevant information about the wave system. For instance, it has been shown in Ref. [86] that dissipative effects occurring in a water tank produce some slow modulation of the spectral (IST) portrait of the Peregrine soliton recorded in water wave experiments reported in Ref. [92]. More recently the IST has been applied to characterize coherent structures in dissipative nonlinear systems described by the cubic Ginzburg-Landau equation [93].

Here, we apply nonlinear spectral analysis to examine the soliton content of the rectangular wave packets in the propagation regime displayed in Fig. 6. For the sake of simplicity, we only present here the numerical results that are associated with the box of duration $\Delta T_2 = 45$ s (central box in Fig. 6). As described in Sec. IV B and also more in detail in Refs. [77,86], the determination of the discrete IST eigenvalues relies on the numerical resolution of Eq. (9) for the potentials ψ_0 that are measured in the experiment.

Figure 7(a) shows the rectangular envelope of the central box of Fig. 6 that has been measured at $z_1 = 6$ m, close to the wave maker. Figure 7(b) shows the corresponding discrete IST spectrum which is composed of seven eigenvalues located well above the real axis. Let us recall that the discrete IST spectrum of the same box was only composed of five eigenvalues in the regime where the dynamics was described by the integrable focusing 1D-NLSE, see Sec. IV B. The result of an increased nonlinearity is therefore that the number of solitons embedded within the box has
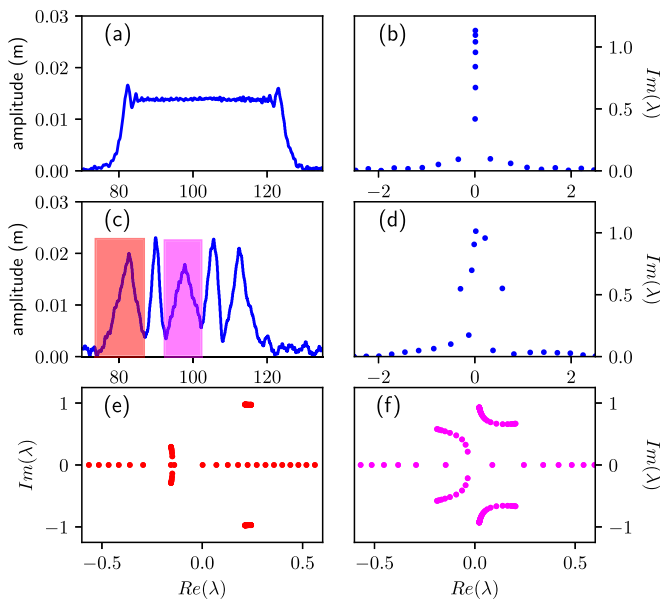
FIG. 7. (a) Envelope of the central wave packet of Fig. 6 measured at $z_1 = 6$ m, close to the wave maker. (b) Discrete IST spectrum of the wave field plotted in (a). (c) Envelope of the central wave packet of Fig. 6 measured at $z_{20} = 120$ m, far from the wave maker. (d) Discrete IST spectrum of the wave field plotted in (c). (e) Local IST spectrum of the coherent structure highlighted in red in (c). (f) Local IST spectrum of the coherent structure highlighted in magenta in (c).

increased, which is not that surprising but which is here substantiated and quantified with the IST.

Figure 7(c) shows the envelope of the central box of Fig. 6 that has been measured at $z_{20} = 120$ m, far from the wave maker. Figure 7(d) shows the corresponding discrete IST spectrum. Comparing Figs. 7(d) and 5(d), we obtain the clear signature that higher-order effects significantly perturbate the discrete IST spectrum (i.e., the soliton content of the rectangular wave packet). Six eigenvalues well above the real axis are observed instead of seven near the wave maker; see Fig. 7(a). Moreover, the real parts of most of these eigenvalues become nonzero which means that the solitons embedded within the box have acquired some velocity, a feature that is fully compatible with the fact that the rectangular box exhibits some slow drift in the space-time plot; see Fig. 6.

To investigate the change of the genus [60] of the coherent structures emerging in the space-time evolution shown in Fig. 6, we have used the tools of local IST analysis introduced in Ref. [77] and already applied for the analysis of experimental signals in Ref. [86]. In the approach used for local IST analysis, the analyzed coherent structure is isolated by truncating the wave profile over some given time interval. The truncated wave field is then periodized in time. This produces some local finite-band approximation of the wave field which can be interpreted within the framework of finite gap theory [75,94,95]. Numerically solving Eq. (9) for the periodized potential ψ_0, we obtain a spectrum that is composed of bands. The number N of bands composing the nonlinear spectrum determines the genus $g = N - 1$ of the solution that can be viewed as a measure of complexity of the space-time evolution of the considered solution.

Figure 7(e) shows the local IST spectrum of the peaked structure highlighted in red in Fig. 7(c) and located at the left-edge of the box. Rigorously speaking the spectrum is composed of three bands but the small-amplitude band crossing the real axis can be seen as being perturbative. Therefore, the local IST spectrum can be seen as being mainly composed of two complex conjugate bands, confirming the nearly genus 1 nature (solitonlike) of the structure analyzed at the left edge of

the box. Note that the spectrum plotted in Fig. 7(e) is qualitatively very similar to the spectrum computed in Fig. 2(e) from numerical simulations of the focusing 1D-NLSE.

Figure 7(f) shows the local IST spectrum of the peaked structure highlighted in magenta in Fig. 7(c) and located in the center of the box. This spectrum is composed of three main bands confirming that the observed object represents a coherent structure of genus 2 (i.e., of breather type). Note that the spectrum plotted in Fig. 7(f) is qualitatively similar to the spectrum computed in Fig. 2(f) from numerical simulations of the focusing 1D-NLSE. Contrary to Fig. 2(f), the spectrum of Fig. 7(f) presents a marked asymmetry that we interpret as arising from the higher-order effects that perturb the integrable dynamics.

VI. SUMMARY AND CONCLUSION

In this paper, we have reported experiments showing the evolution of nonlinear deep-water surface gravity waves having their initial envelopes in the form of large-scale near-rectangular barriers. We have shown that nonlinear wave packets are not necessarily disintegrated by the Benjamin-Feir instability and that there exist some regimes in which a specific, strongly nonlinear modulation, propagates from the edges of the wave packet toward the center with finite speed. The observed counter-propagating dispersive dam break flows represent modulated nonlinear wave trains that can be described within the framework of the semiclassical 1D-NLSE. They could be viewed as examples of DSW dynamics persisting in focusing (modulationally unstable) nonlinear media.

Our experimental results are shown to be in good quantitative agreement with predictions of the 1D-NLSE semiclassical theory [60,61], confirming the robustness of the observed dynamical scenario with respect to perturbative higher-order nonlinear effects inevitably present in a water wave experiment. We have also shown that nonlinear spectral analysis [86] can be used to advantage to determine the soliton content of the generated wave packets while also providing useful information about the local wave dynamics in terms of the number of fundamental nonlinear wave modes (the genus) comprising the observed structure at a given space-time point.

By confirming that DSW dynamics can be observed in deep water waves, our work opens way to further experimental and theoretical investigations on the subject of DSW formation in focusing nonlinear media. In particular, several scenarios [52] associated with the so-called Riemann problems—i.e., the evolution of a jump discontinuities (not necessarily dam breaks) between two uniform states of the initial field—could be also possibly observed in deep water waves.

Interesting questions are related to the competition between the DSW formation and the Benjamin-Feir instability. Our experiments are performed in a regime where the DSW dynamics plays the dominating role and the effects of the Benjamin-Feir instability can be neglected, but it would be interesting to examine in detail how the Benjamin-Feir instability affects the DSW structure at longer propagation times. Finally, our experiments have shown that the generated DSWs exhibit certain robustness to higher-order nonlinear effects. It is another interesting and challenging question to investigate these higher order effects more in detail from the theoretical perspective.

ACKNOWLEDGMENTS

APPENDIX: FINITE DEPTH EFFECTS

As shown in Ref. [96] the weakly nonlinear, narrow-banded approximation of the fully nonlinear irrotational and inviscid water wave equations is the 1D-NLSE under the following form:

$$\frac{\partial A}{\partial t} + \frac{1}{2}\frac{\omega_0}{k_0}\nu\frac{\partial A}{\partial z} + i\frac{1}{8}\frac{\omega_0}{k_0^2}\kappa\frac{\partial^2 A}{\partial z^2} + i\frac{1}{2}\omega_0 k_0^2 \gamma|A|^2 A = 0, \tag{A1}$$

where A is the complex envelope of the water wave. ν is the correction to the group velocity for finite depth. κ and γ are coefficients that in general depend on the water depth h at the dominant wave number k_0 and at the corresponding angular frequency ω_0.

The general expressions of ν, κ, and γ are given by (see, e.g., Ref. [66], and see Ref. [96] for the derivation)

$$\nu = 1 + \frac{2k_0 h}{\sinh(2k_0 h)}, \tag{A2}$$

$$\kappa = -\nu^2 + 2 + 8(k_0 h)^2 \frac{\cosh(2k_0 h)}{\sinh^2(2k_0 h)}, \tag{A3}$$

$$\gamma = \frac{\cosh(4k_0 h) + 8 - 2\tanh^2(k_0 h)}{8\sinh^4(k_0 h)},$$

$$-\frac{(2\cosh^2(k_0 h) + 0.5\nu)^2}{\sinh^2(2k_0 h)}\left(\frac{k_0 h}{\tanh(k_0 h)} - \frac{\nu^2}{4}\right). \tag{A4}$$

For a hydrodynamic wave-maker problem, it is convenient to use the 1D-NLSE in the form of an evolution equation in space. Using changes of variables described in Refs. [75,97], one obtains the following evolution equation:

$$i\frac{\partial A}{\partial z} + \frac{\kappa}{\nu^3}\frac{k_0}{\omega_0^2}\frac{\partial^2 A}{\partial t^2} + \frac{\gamma}{\nu}k_0^3|A|^2 A = 0, \tag{A5}$$

in the frame of reference moving with the group velocity of the wave packets.

In the experiments reported in Fig. 1(b), the numerical value of $k_0 h$ is 12.3 and the numerical values of the corrective terms ν and κ given by Eqs. (A2) and (A3) are very close to unity. However, the numerical value of γ is ~ 0.91 which means that the finite-depth correction to the cubic nonlinearity is small but not negligible. Therefore, our experiments are described by Eq. (A5) in which the values of the corrective terms are set to $\kappa = \nu = 1$ and $\gamma = \alpha = 0.91$.

---

[1] G. B. Whitham and M. J. Lighthill, Nonlinear dispersive waves, Proc. R. Soc. London A **283**, 238 (1965).

[2] M. J. Lighthill, Contributions to the theory of waves in nonlinear dispersive systems, IMA J. Appl. Math. **1**, 269 (1965).

[3] T. B. Benjamin and J. E. Feir, The disintegration of wave trains on deep water part 1. theory, J. Fluid Mech. **27**, 417 (1967).

[4] T. B. Benjamin, Instability of periodic wave trains in nonlinear dispersive systems, Proc. R. Soc. London A **299**, 59 (1967).

[5] B. M. Lake, H. C. Yuen, H. Rungaldier, and W. E. Ferguson, Nonlinear deep-water waves: Theory and experiment. Part 2. Evolution of a continuous wave train, J. Fluid Mech. **83**, 49 (1977).

[6] M. S. Longuet-Higgins, Modulation of the amplitude of steep wind waves, J. Fluid Mech. **99**, 705 (1980).

[7] W. K. Melville, The instability and breaking of deep-water waves, J. Fluid Mech. **115**, 165 (1982).

[8] M.-Y. Su, M. Bergin, P. Marler, and R. Myrick, Experiments on nonlinear instabilities and evolution of steep gravity-wave trains, J. Fluid Mech. **124**, 45 (1982).

[9] M.-Y. Su, Evolution of groups of gravity waves with moderate to high steepness, Phys. Fluids **25**, 2167 (1982).

[10] V. E. Zakharov, Stability of periodic waves of finite amplitude on the surface of a deep fluid, J. Appl. Mech. Tech. Phys. **9**, 190 (1968).

[11] D. J. Benney and A. C. Newell, The propagation of nonlinear wave envelopes, J. Math. Phys. **46**, 133 (1967).

[12] L. I. Zagryadskaya and L. A. Ostrovskii, Observed self-influence of modulated waves in a nonlinear line, Radiophys. Quant. Electron. **11**, 548 (1968).

[13] L. A. Ostrovskii and L. V. Soustov, Selfmodulation of electromagnetic waves in nonlinear transmission lines, Radiophys. Quant. Electron. **15**, 182 (1972).

[14] V. E. Zakharov and L. A. Ostrovsky, Modulation instability: The beginning, Physica D: Nonlin. Phenom. **238**, 540 (2009).

[15] K. E. Strecker, G. B. Partridge, A. G. Truscott, and R. G. Hulet, Formation and propagation of matter-wave soliton trains, Nature **417**, 150 (2002).

[16] D. Kip, M. Soljacic, M. Segev, E. Eugenieva, and D. N. Christodoulides, Modulation instability and pattern formation in spatially incoherent light beams, Science **290**, 495 (2000).

[17] K. Tai, A. Hasegawa, and A. Tomita, Observation of Modulational Instability in Optical Fibers, Phys. Rev. Lett. **56**, 135 (1986).

[18] M. Soljacic, M. Segev, T. Coskun, D. N. Christodoulides, and A. Vishwanath, Modulation Instability of Incoherent Beams in Noninstantaneous Nonlinear Media, Phys. Rev. Lett. **84**, 467 (2000).

[19] D. R. Solli, G. Herink, B. Jalali, and C. Ropers, Fluctuations and correlations in modulation instability, Nat. Photon. **6**, 463 (2012).

[20] C. Sun, L. Waller, D. V. Dylov, and J. W. Fleischer, Spectral Dynamics of Spatially Incoherent Modulation Instability, Phys. Rev. Lett. **108**, 263902 (2012).

[21] J. Meier, G. I. Stegeman, D. N. Christodoulides, Y. Silberberg, R. Morandotti, H. Yang, G. Salamo, M. Sorel, and J. S. Aitchison, Experimental Observation of Discrete Modulational Instability, Phys. Rev. Lett. **92**, 163902 (2004).

[22] S. Mosca, M. Parisi, I. Ricciardi, F. Leo, T. Hansson, M. Erkintalo, P. Maddaloni, P. De Natale, S. Wabnitz, and M. De Rosa, Modulation Instability Induced Frequency Comb Generation in a Continuously Pumped Optical Parametric Oscillator, Phys. Rev. Lett. **121**, 093903 (2018).

[23] M. Erkintalo, K. Hammani, B. Kibler, C. Finot, N. Akhmediev, J. M. Dudley, and G. Genty, Higher-Order Modulation Instability in Nonlinear Fiber Optics, Phys. Rev. Lett. **107**, 253901 (2011).

[24] B. Kibler, J. Fatome, C. Finot, G. Millot, F. Dias, G. Genty, N. Akhmediev, and J. M. Dudley, The peregrine soliton in nonlinear fibre optics, Nat. Phys. **6**, 790 (2010).

[25] B. Frisquet, B. Kibler, and G. Millot, Collision of Akhmediev Breathers in Nonlinear Fiber Optics, Phys. Rev. X **3**, 041032 (2013).

[26] N. Akhmediev and A. Ankiewicz, Modulation instability, Fermi-Pasta-Ulam recurrence, rogue waves, nonlinear phase shift, and exact solutions of the Ablowitz-Ladik equation, Phys. Rev. E **83**, 046603 (2011).

[27] O. Kimmoun, H. Hsu, H. Branger, M. S. Li, Y. Y. Chen, C. Kharif, M. Onorato, E. J. R. Kelleher, B. Kibler, N. Akhmediev, and A. Chabchoub, Modulation instability and phase-shifted Fermi-Pasta-Ulam recurrence, Sci. Rep. **6**, 28516 (2016).

[28] A. Mussot, C. Naveau, M. Conforti, A. Kudlinski, F. Copie, P. Szriftgiser, and S. Trillo, Fibre multiwave mixing combs reveal the broken symmetry of Fermi–Pasta–Ulam recurrence, Nat. Photon. **12**, 303 (2018).

[29] V. E. Zakharov and A. A. Gelash, Nonlinear Stage of Modulation Instability, Phys. Rev. Lett. **111**, 054101 (2013).

[30] A. A. Gelash and V. E. Zakharov, Superregular solitonic solutions: A novel scenario for the nonlinear stage of modulation instability, Nonlinearity **27**, R1 (2014).

[31] B. Kibler, A. Chabchoub, A. Gelash, N. Akhmediev, and V. E. Zakharov, Superregular Breathers in Optics and Hydrodynamics: Omnipresent Modulation Instability Beyond Simple Periodicity, Phys. Rev. X **5**, 041026 (2015).

[32] G. Biondini and D. Mantzavinos, Universal Nature of the Nonlinear Stage of Modulational Instability, Phys. Rev. Lett. **116**, 043902 (2016).

[33] G. Biondini, S. Li, and D. Mantzavinos, Oscillation structure of localized perturbations in modulationally unstable media, Phys. Rev. E **94**, 060201 (2016).

[34] G. Biondini and D. Mantzavinos, Long-time asymptotics for the focusing nonlinear Schrödinger equation with nonzero boundary conditions at infinity and asymptotic stage of modulational instability, Commun. Pure Appl. Math. **70**, 2300 (2017).

[35] A. E. Krach, P. Suret, G. El, and S. Randoux, Nonlinear Evolution of the Locally Induced Modulational Instability in Fiber Optics, Phys. Rev. Lett. **122**, 054101 (2019).

[36] M. Conforti, S. Li, G. Biondini, and S. Trillo, Auto-modulation versus breathers in the nonlinear stage of modulational instability, Opt. Lett. **43**, 5291 (2018).

[37] V. E. Zakharov, Turbulence in integrable systems, Stud. Appl. Math. **122**, 219 (2009).

[38] S. Randoux, P. Walczak, M. Onorato, and P. Suret, Intermittency in Integrable Turbulence, Phys. Rev. Lett. **113**, 113902 (2014).

[39] P. Walczak, S. Randoux, and P. Suret, Optical Rogue Waves in Integrable Turbulence, Phys. Rev. Lett. **114**, 143903 (2015).

[40] D. S. Agafontsev and V. E. Zakharov, Integrable turbulence and formation of rogue waves, Nonlinearity **28**, 2791 (2015).

[41] E. Pelinovsky and A. S. Kokorina, Numerical modeling of the KdV random wave field, Eur. J. Mech. B/Fluids **25**, 425 (2006).

[42] J. M. Soto-Crespo, N. Devine, and N. Akhmediev, Integrable Turbulence and Rogue Waves: Breathers or Solitons? Phys. Rev. Lett. **116**, 103901 (2016).

[43] P. Suret, R. El Koussaifi, A. Tikan, Cl. Evain, S. Randoux, C. Szwaj, and S. Bielawski, Single-shot observation of optical rogue waves in integrable turbulence using time microscopy, Nat. Commun. **7**, 13136 (2016).

[44] S. Randoux, F. Gustave, P. Suret, and G. El, Optical Random Riemann Waves in Integrable Turbulence, Phys. Rev. Lett. **118**, 233901 (2017).

[45] A. Tikan, S. Bielawski, C. Szwaj, S. Randoux, and P. Suret, Single-shot measurement of phase and amplitude by using a heterodyne time-lens system and ultrafast digital time-holography, Nat. Photonics **12**, 228 (2018).

[46] A. Cazaubiel, G. Michel, S. Lepot, B. Semin, S. Aumaître, M. Berhanu, F. Bonnefoy, and E. Falcon, Coexistence of solitons and extreme events in deep water surface waves, Phys. Rev. Fluids **3**, 114802 (2018).

[47] A. E. Krach, D. Agafontsev, S. Randoux, and P. Suret, Statistical Properties of the Nonlinear Stage of Modulation Instability in Fiber Optics, Phys. Rev. Lett. **123**, 093902 (2019).

[48] M. Bertola and A. Tovbis, Universality for the focusing nonlinear Schrödinger equation at the gradient catastrophe point: Rational breathers and poles of the tritronquée solution to Painlevé I, Commun. Pure Appl. Math. **66**, 678 (2013).

[49] A. Tikan, C. Billet, G. El, A. Tovbis, M. Bertola, T. Sylvestre, F. Gustave, S. Randoux, G. Genty, P. Suret, and J. M. Dudley, Universality of the Peregrine Soliton in the Focusing Dynamics of the Cubic Nonlinear Schrödinger Equation, Phys. Rev. Lett. **119**, 033901 (2017).

[50] L. Shemer, E. Kit, and H. Jiao, An experimental and numerical study of the spatial evolution of unidirectional nonlinear water-wave groups, Phys. Fluids **14**, 3380 (2002).

[51] A. Chabchoub, N. Hoffmann, M. Onorato, G. Genty, J. M. Dudley, and N. Akhmediev, Hydrodynamic Supercontinuum, Phys. Rev. Lett. **111**, 054104 (2013).

[52] G. Biondini, Riemann problems and dispersive shocks in self-focusing media, Phys. Rev. E **98**, 052220 (2018).

[53] G. A. El and M. A. Hoefer, Dispersive shock waves and modulation theory, Physica D: Nonlin. Phenom. **333**, 11 (2016), dispersive Hydrodynamics.

[54] G. B. Whitham, *Linear and Nonlinear Waves*, Vol. 42 (John Wiley & Sons, New York, 2011).

[55] D. H. Peregrine, Calculations of the development of an undular bore, J. Fluid Mech. **25**, 321 (1966).

[56] T. B. Benjamin and M. J. Lighthill, On cnoidal waves and bores, Proc. R. Soc. London A **224**, 448 (1954).

[57] J. Fatome, C. Finot, G. Millot, A. Armaroli, and S. Trillo, Observation of Optical Undular Bores in Multiple Four-Wave Mixing, Phys. Rev. X **4**, 021022 (2014).

[58] G. Xu, A. Mussot, A. Kudlinski, S. Trillo, F. Copie, and M. Conforti, Shock wave generation triggered by a weak background in optical fibers, Opt. Lett. **41**, 2656 (2016).

[59] G. Xu, M. Conforti, A. Kudlinski, A. Mussot, and S. Trillo, Dispersive Dam-Break Flow of a Photon Fluid, Phys. Rev. Lett. **118**, 254101 (2017).

[60] G. A. El, E. G. Khamis, and A. Tovbis, Dam break problem for the focusing nonlinear Schrödinger equation and the generation of rogue waves, Nonlinearity **29**, 2798 (2016).

[61] R. Jenkins and K. D. McLaughlin, Semiclassical limit of focusing NLS for a family of square barrier initial data, Comm. Pure Appl. Math. **67**, 246 (2014).

[62] A. Chabchoub, G. Genty, J. M. Dudley, B. Kibler, and T. Waseda, Experiments on spontaneous modulation instability in hydrodynamics, in *Proceedings of The Twenty-Seventh (2017) International Ocean and Polar Engineering Conference, San Francisco* (ISOPE, Cupertino, 2017), ISOPE-I-17-582, pp. 420–424.

[63] See Supplemental Material at http://link.aps.org/supplemental/10.1103/PhysRevFluids.5.034802 for a set of videos of the experiments and of the simulations, as well as further experimental results on the Fourier analysis of experimental data.

[64] H.-H. Hwung, W.-S. Chiang, and S.-C. Hsiao, Observations on the evolution of wave modulation, Proc. R. Soc. A **463**, 85 (2007).

[65] M. P. Tulin and T. Waseda, Laboratory observations of wave group evolution, including breaking effects, J. Fluid Mech. **378**, 197 (1999).

[66] L. Shemer and B. K. Ee, Steep unidirectional wave groups—Fully nonlinear simulations vs. experiments, Nonlin. Process. Geophys. **22**, 737 (2015).

[67] D. Weisman, S. Fu, M. Gonçalves, L. Shemer, J. Zhou, W. P. Schleich, and A. Arie, Diffractive Focusing of Waves in Time and in Space, Phys. Rev. Lett. **118**, 154301 (2017).

[68] S. A. Akhmanov, A. P. Sukhorukov, and R. V. Khokhlov, Self-focusing and diffraction of light in a nonlinear medium, Soviet Physics Uspekhi **10**, 609 (1968).

[69] S. V. Manakov, On the theory of two-dimensional stationary self-focusing of electromagnetic waves, Zh. Eksp. Tecr. Fiz. **65**, 505 (1973) [Sov. Phys. JETP **38**, 505 (1974)].

[70] S. V. Manakov, Nonlinear Fraunhofer diffraction, Zh. Eksp. Toor. Fiz. **65**, 1392 (1973) [Sov. Phys.-JETP **38**, 693 (1974)].

[71] W. Wan, D. V. Dylov, C. Barsi, and J. W. Fleischer, Diffraction from an edge in a self-focusing medium, Opt. Lett. **35**, 2819 (2010).

[72] G. Marcucci, D. Pierangeli, A. J. Agranat, R.-K. Lee, E. DelRe, and C. Conti, Topological control of extreme waves, Nat. Commun. **10**, 5090 (2019).

[73] F. Audo, B. Kibler, J. Fatome, and C. Finot, Experimental observation of the emergence of peregrine-like events in focusing dam break flows, Opt. Lett. **43**, 2864 (2018).

[74] G. Biondini, G. A. El, M. A. Hoefer, and P. D. Miller, Dispersive hydrodynamics: Preface, Physica D: Nonlin. Phenom. **333**, 1 (2016).

[75] A. Osborne, *Nonlinear Ocean Waves* (Academic Press, San Diego, 2010).

[76] J. M. Dudley, F. Dias, M. Erkintalo, and G. Genty, Instabilities, breathers, and rogue waves in optics, Nat. Photon. **8**, 755 (2014).

[77] S. Randoux, P. Suret, and G. El, Inverse scattering transform analysis of rogue waves using local periodization procedure, Sci. Rep. **6**, 29238 (2016).

[78] G. A. El, A. V. Gurevich, V. V. Khodorovskii, and A. L. Krylov, Modulational instability and formation of a nonlinear oscillatory structure in a"focusing"medium, Phys. Lett. A **177**, 357 (1993).

[79] A. M. Kamchatnov, New approach to periodic solutions of integrable equations and nonlinear theory of modulational instability, Phys. Rep. **286**, 199 (1997).

[80] G. Biondini, S. Li, D. Mantzavinos, and S. Trillo, Universal behavior of modulationally unstable media, SIAM Rev. **60**, 888 (2018).

[81] D. S. Agafontsev and V. E. Zakharov, Integrable turbulence generated from modulational instability of cnoidal waves, Nonlinearity **29**, 3551 (2016).

[82] M. V. Pavlov, Nonlinear Schrödinger equation and the Bogolyubov-Whitham method of averaging, TMF **71**, 351 (1987) [Theor. and Math. Phys. **71**, 584 (1987)].

[83] M. G. Forest and J.-E. Lee, Geometry and modulation theory for the periodic nonlinear Schrodinger equation, in *Oscillation Theory, Computation, and Methods of Compensated Compactness*, edited by C. Dafermos, J. L. Ericksen, D. Kinderlehrer, and M. Slemrod (Springer, New York, NY, 1986), pp. 35–70.

[84] A. Tovbis and G. A. El, Semiclassical limit of the focusing NLS: Whitham equations and the Riemann–Hilbert problem approach, Physica D: Nonlin. Phenom. **333**, 171 (2016).

[85] E. D. Belokolos, A. I. Bobenko, V. Z. Enolski, A. R. Its, and V. B. Matveev, *Algebro-geometric Approach to Nonlinear Integrable Equations* (Springer, New York, 1994).

[86] S. Randoux, P. Suret, A. Chabchoub, B. Kibler, and G. El, Nonlinear spectral analysis of peregrine solitons observed in optics and in hydrodynamic experiments, Phys. Rev. E **98**, 022219 (2018).

[87] V. E. Zakharov and A. B. Shabat, Exact theory of two-dimensional self-focusing and one-dimensional self-modulation of waves in nonlinear media, Sov. Phys. JETP **34**, 62 (1972).

[88] J. Burzlaff, The soliton number of optical soliton bound states for two special families of input pulses, J. Phys. A: Math. Gen. **21**, 561 (1988).

[89] Y. S. Kivshar, On the soliton generation in optical fibres, J. Phys. A: Math. Gen. **22**, 337 (1989).

[90] E. V. Sedov, A. A. Redyuk, M. P. Fedoruk, A. A. Gelash, L. L. Frumin, and S. K. Turitsyn, Soliton content in the standard optical OFDM signal, Opt. Lett. **43**, 5985 (2018).

[91] J. Yang, *Nonlinear Waves in Integrable and Nonintegrable Systems*, Mathematical Modeling and Computation (Society for Industrial and Applied Mathematics, Philadelphia, PA, 2010).

[92] A. Chabchoub, N. P. Hoffmann, and N. Akhmediev, Rogue Wave Observation in a Water Wave Tank, Phys. Rev. Lett. **106**, 204502 (2011).

[93] I. S. Chekhovskoy, O. V. Shtyrina, M. P. Fedoruk, S. B. Medvedev, and S. K. Turitsyn, Nonlinear Fourier Transform for Analysis of Coherent Structures in Dissipative Systems, Phys. Rev. Lett. **122**, 153901 (2019).

[94] E. R. Tracy, H. H. Chen, and Y. C. Lee, Study of Quasiperiodic Solutions of the Nonlinear Schrödinger Equation and the Nonlinear Modulational Instability, Phys. Rev. Lett. **53**, 218 (1984).

[95] P. G. Grinevich and P. M. Santini, The finite gap method and the analytic description of the exact rogue wave recurrence in the periodic NLS Cauchy problem, Nonlinearity **31**, 5258 (2018).

[96] C. C. Mei, *The Applied Dynamics of Ocean Surface Waves* (World Scientific, Singapore, 1992).

[97] A. Chabchoub and R. H. J. Grimshaw, The hydrodynamic nonlinear Schrodinger equation: Space and time, Fluids **1**, 23 (2016).